International Journal of Micro Air Vehicles

Article

International Journal of Micro Air Vehicles
2016, Vol. 8(3) 181–193

DOI: 10.1177/1756829316667770
mav.sagepub.com

SAGE

Experimental investigation on flow characteristics of a four-wing micro air vehicle

Lisong Shi[1], Chunkit Uy[1], Shih K Huang[2], Zifeng Yang[2], George PG Huang[2] and Chihyung Wen[1]

Abstract

The aim of current research work on micro air vehicles is to realize their autonomous control, i.e. building a library for a lookup table that would apply to micro electronics. In doing so, comprehensive flight tests need to be carried out. In this study, a four-wing flapping MAV is built and a multi-discipline approach is used to design the MAV model. Precision manufacturing technology is introduced here. The finished micro air vehicle has a weight of 8 g and is tested for flight by remote control. The micro air vehicle can perform both hovering and forward flight with high maneuverability. Forward flight is investigated first in this paper. Particle image velocimetry system is employed to examine unsteady aerodynamic performance in selected flight conditions. The study reveals that the micro air vehicle model will provide enough lift at a 30° angle of attack and flapping frequency of 12 Hz, which is consistent with real-life forward flight observations.

Keywords

Four-wing MAV, Particle image velocimetry, Precision technology, Flapping mechanism, Forward flight

Date received: 9 October 2015; accepted: 2 February 2016

Introduction

Flapping wing micro air vehicles (MAVs) have attracted attentions from a variety of research fields in recent years. Exceptional maneuverability and low noise generation are key features of flapping wing MAVs and they are ideal for executing missions that are too difficult or dangerous for humans, such as searching for radiation leaks in nuclear plants, or survivors in a fire. These kinds of missions, i.e. intelligence, surveillance, and reconnaissance, are often used in urban and indoor environments, which require a small-sized vehicle that can be automatically controlled.

To build the preliminary design of a flapping-flight vehicle, Liu[1] suggested the use of scaling laws that model the characteristics of natural flapping and fixed-wing flyers (i.e. the wingspan, chord, etc.). Besides, the flight characteristics of insects and hummingbirds have been the inspiration and drive for constructing new MAVs, and biologists who carried out related studies[2–5] have revealed that clap and fling is the primary mechanism behind the flight of small natural flyers. Tien et al.[6] suggested that the ground effect is dominant for the initial flight of insects, and considered the flight of the beetle as their model.

Many research groups[7–13] around the world have tried to develop their own MAVs and studied flow characteristics of related models. Nakata et al.[7] and Croon et al.[8] built a four-wing flapper with the use of the clap and fling mechanism, whereas Pornsin-Sirirak et al.[9] and Nguyen et al.[10] applied microelectromechanical systems (MEMS) technology and a lightweight piezoelectric composite actuator (LIPCA) to build their MAV, respectively. Jones et al.[11] developed a

[1]Department of Mechanical Engineering, The Hong Kong Polytechnic University, Hong Kong, PR China
[2]Department of Mechanical and Materials Engineering, Wright State University, Dayton, OH, USA

Corresponding author:
Chihyung Wen, Department of Mechanical Engineering, The Hong Kong Polytechnic University, Hong Kong, PR China.
Email: cywen@polyu.edu.hk

fixed-wing MAV activated by a clapping tail thruster, and both Banala et al.[12] and McIntosh et al.[13] focused on the development of two-wing flapping MAVs. Both wind tunnel experiments[7–11] and force measurements[7–13] play important roles in their studies, and those are also used in the work of this paper.

Wing flexibility, wing structure, and wing membrane materials are taken into consideration when building a highly maneuverable MAV. Heathcote et al.[14] discovered that wing flexibility is one of the important factors that influence the thrust generation from flapping wings, and Yusoff et al.[15] found that the degree of flexibility is unique with different flapping speeds. Wu et al.[16] showed that the thrust force produced during flapping depends on the cross-strut pattern on the wings. Hu et al.[17] used nylon and latex as material to make flexible wings and compared their aerodynamic performance with that of a conventional rigid wing. They found that nylon wings with medium flexibility among the three shows the best aerodynamic performance. Nanang et al.[18] explored the implementation of wing feather separation and lead lagging motion to a flapping wing by constructing an outer wing separation design.

Wing deformation is primarily driven by inertial loads rather than aerodynamic loads.[19] To determine the contribution from inertial loads in the total lift force measured, two approaches are proposed by researchers: mathematical modeling or experimental studies. Isaac et al.[20] found that instantaneous inertial forces that act on flapping wings can be a function of the mass of the test wing, flapping frequency, and angular displacement. Based on the work of Isaac et al.[20] and Hu et al.,[17] the time-averaged mean inertial force can be expressed as

$$F_{inertial} \propto CMf^2 \tag{1}$$

where C is the characteristic parameter of the flapping motion, M is the mass of the flapping wing, and f is the flapping frequency. By flapping the wings without skin (i.e. assume there is almost no aerodynamic force), the inertial force can then be estimated.[17] Their result revealed that the inertial force contributes to less than 5.0% of the measured aerodynamic forces.[17] Another approach is to measure the mean inertial lift forces by putting the wing model into a vacuum chamber, as suggested by Nguyen et al.[10] and Wu et al.[16] Nguyen et al.[10,21] found that the vertical inertial force measured at a vacuum level of 95% for a flapper can be almost zero on average. Based on their studies, it is considered that inertial forces on the flapper have little to do with the measured aerodynamic forces, and will not be examined in detail in this study.

In this paper, a wing model similar to that proposed in Huang et al.[22] is applied during the fabrication of the MAV and a flight test is conducted with a remote control. Details of the design and manufacture of the MAV model are discussed in the subsequent section. The aim of current research work on MAVs is to realize their autonomous control, i.e. building a library for a lookup table that would apply to micro electronics, and possibly include the use of sensors. In doing so, a comprehensive understanding of the MAV flight is required, including both hovering and forward flight conditions. In the following section, the forward flight of a MAV is used as an example and examined. The wing model is placed into a wind tunnel for force measurement with a range of angles of attack and different flapping frequencies. A freestream velocity of 2 m/s is established in the wind tunnel, which acts as gusty wind that may be encountered by a MAV in the air during measurement. Particle image velocimetry (PIV) system is employed to demonstrate the flow physics under those flight conditions.

The aim of the present work is to help to solidify knowledge on the construction of small-sized flapping air vehicles. Specifically, the biplane wing configuration is crucial to the aerodynamic performance of MAVs.[7,8] Therefore, by conducting a series of experiments on aerodynamic measurements, the feasibility of the model is proven in real-life forward flight. The result obtained in this work provides insight towards design improvements for flapping MAVs, and with the integration of automatic control in the future, a high-performing MAV is expected to be manufactured which can benefit the community.

Method and materials

Model

Design and manufacturing. A four-wing MAV model was designed and tested for flight (see section "Flight testing"). It has a weight of 8 g with a wingspan of 200 mm and chord length of 60 mm. The maximum stroke angle is 110° and the model has the capability of flapping up to a frequency of 15 Hz. Based on the research of other academics,[7,8] a biplane model is considered to be more suitable for constructing the MAV, as the low amplitude rocking of the fuselage in flight can provide a stable platform for camera recording.

The flapping motion was executed by using a double-gear crank-rocker mechanism, with a double gear reduction of about 27:1. Gearotic Motion software was used for the design of the gear ratio. The resultant file could be directly opened in Solidworks for further alterations. In this model, the clap and fling mechanism

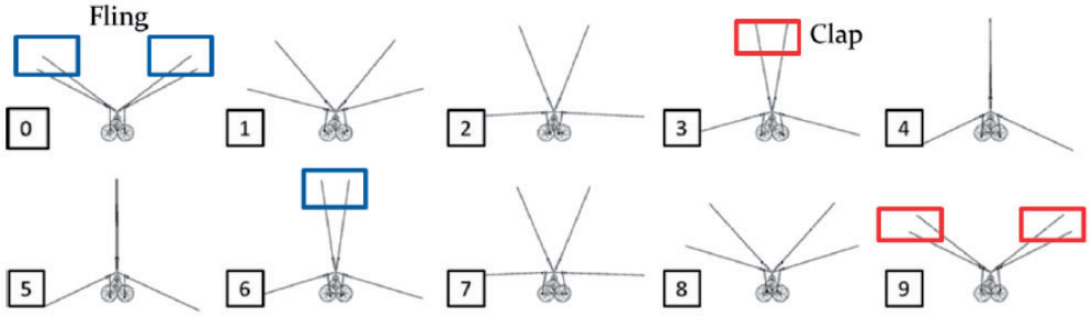

Figure 1. Front view of the wing configuration of MAV model at successive moment in one flapping cycle.

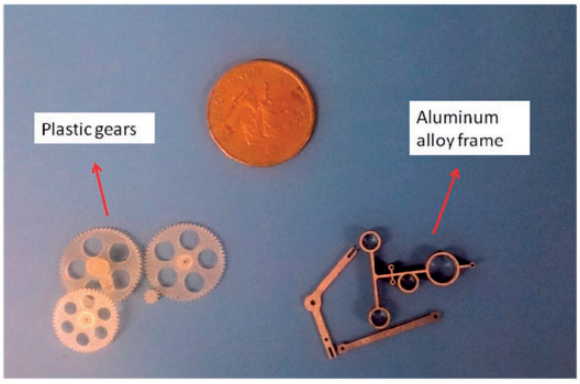

Figure 2. Plastic gears made by rapid prototyping machining (left). Aluminum alloy parts made by electric discharge machining (right). Diameter of dime (HKD) = 25 mm (top) used as reference for size.

Table 1. List of parts used in constructing MAV.

Item	Weight (g)	
Receiver board with actuator (MX-Rx42H)	2.59	
3.7 V 70 mAh batteries	(Eflite)	2.65
Brushless motor	1.33	
Double-gear crank-rocker (Total)	2.32	
Wings with strut pattern × 2 (Total)	1.1	
Fuselage	0.94	
Total (without batteries)	8.28	

is applied. This mechanism was first proposed by Weis–Fogh in 1973,[5] which was used to describe wing motions of a parasitic wasp, Encarsia, and the idea is now widely applied in MAV design.[7,8] The biplane structure here helps to implement clap and fling three times in one cycle—a pair of wings clap at each side in the beginning of the cycle and the middle two hinges come together at the half cycle (Figure 1). The upper clap and fling motion at the half cycle gives rise to a stronger forward motion of the vehicle.

Precision machinery is the key technology used in the design and manufacturing of this MAV. Electric discharge machining (EDM) was applied to produce the metal parts, like the frame and gear holder (Figure 2). Aluminum-alloy 7075 was used in the production, and the positioning accuracy of the EDM was about ±0.01 mm. The gears in the drive mechanism were made by using ProJet® 3500 HD by 3D Systems with their multi-jet modeling (MJM) technology. This type of rapid prototyping machining produces high resolution gears (i.e. accuracy of 0.025–0.05 mm per 25.4 mm) with apparent strength to withstand the drive motion. The wax (VisiJet S300) is crucial for this rapid prototyping process as it provides support and ensures that the shape of the gears made can be maintained after production. Once the Solidworks drawing was available, the design was then sent to the machine for rapid prototyping.

On considering the wing flexibility, Combes et al.[23] estimated the variation in the flexural stiffness of hawkmoths and dragonflies by using simple mathematical functions. The result revealed that flexural stiffness sharply declines from the wing base to the tip, and the leading edge to the trailing edges.[23] Consequently, it was recommended that the wing should contain a certain degree of flexibility. Thin polyester film is used for the wing membrane in the MAV model in this study because of this reason. A carbon fiber rod (0.7 mm) was introduced onto the wing surface so that different degrees of flexibility could be realized from the wing base to the wing tip.

A receiver board with servos was used as the flight control system on the tail (Figure 4). Both the vertical and horizontal control surfaces were connected to the rudder and elevator servos through a carbon fiber rod (Figure 3). Basic light carbon fiber tubes with two diameters, 0.7 mm and 1 mm, were used to construct the fuselage. The MAV could then achieve both forward and hovering flight with the control of the rudder, elevator at the tail, and the flapping frequency. Table 1 lists the major parts used in constructing the MAV and their corresponding weight.

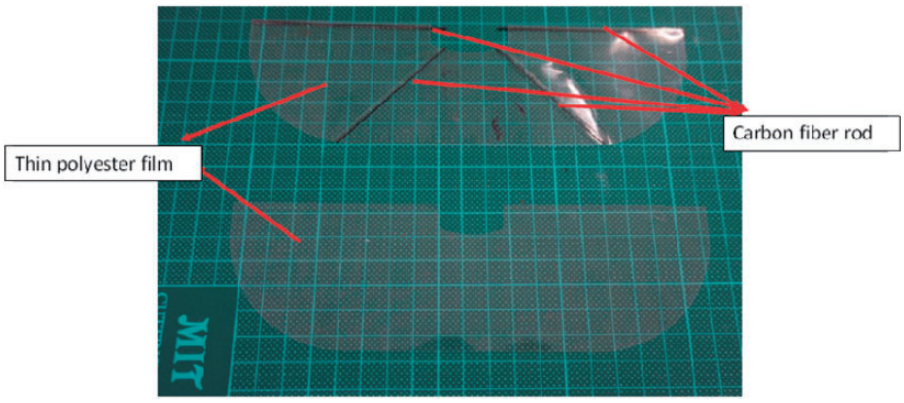

Figure 3. Wing structure with strut pattern on MAV.

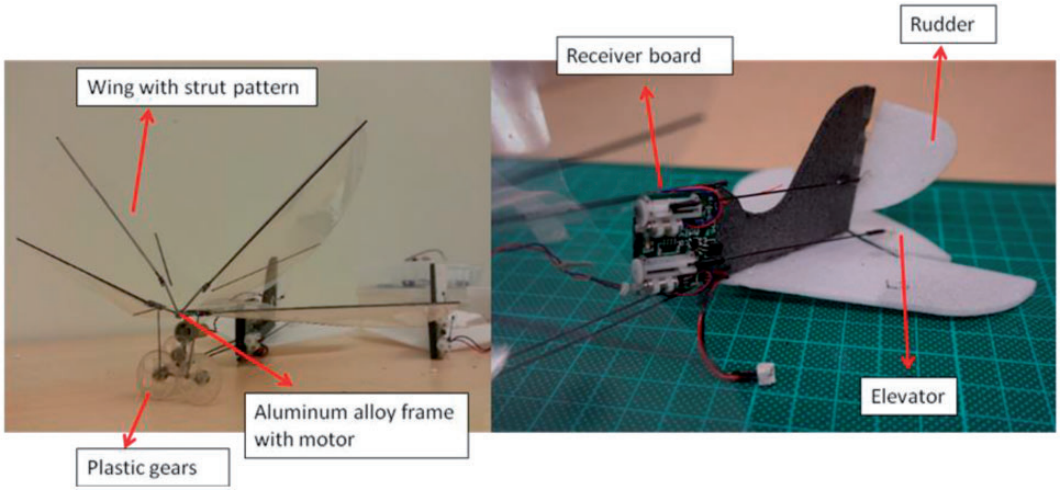

Figure 4. Four-wing micro air vehicle and flight control system on tail.

Flight testing. The flapping MAV presented here has the ability to perform acrobatic moves, such as dashing, rapid turning and hovering (see attached video clip). The maximum speed of the wind gust outdoors is about 2 m/s (the same freestream velocity is chosen in the wind tunnel experiment in the following section for reference). The flying speed of the MAV is can be up to 3 m/s. For forward flight, the MAV can fly more or less at a 30° angle, which correlates to the result in the force measurement test (section "Force measurement under incoming flow"). The angle of attack (AoA) of the MAV is much higher in hovering conditions.

Force measurement under incoming flow

Force measurement was performed under a free stream velocity of 2 m/s in a wind tunnel, which corresponds to outdoor flight conditions in the real forward flight of the MAV (0:08 to 0:10 in the video clip). A low-speed wind tunnel was used in the experiment with a cross-sectional area of 0.6 m × 0.6 m and a maximum velocity of 50 m/s. Honeycomb is installed upstream, rendering a turbulence intensity of less than 0.5%. The corresponding Reynolds number is 13,600, based on a root chord length of 60 mm. The data helped to interpret the flow structure captured in the flow visualization. Kyowa 3-component force transducers LSM-B-SA1 were used in the setup and their accuracy was within 0.5% of the rated output. For data acquisition (DAQ), the DAQ system was connected between the load cell and the computer. The wing model was connected with a 150 mm steel shaft vertically located to the load cell. A DC power supply was installed to control the voltage to actuate the wings and a Monarch PLT200 laser tachometer was used to monitor the flapping frequency of the wings. With different ranges of AoA and flapping frequency set as the parameters, the forces were measured and recorded at a sampling rate of 2000 Hz for 10 s in each trial. Low pass filter was used in signal processing for the force data and the cutoff frequency was 50 Hz. Figure 5 shows the force component on the wing model during measurement.

Flow visualization

A PIV system was used to visualize the flow that was surrounding the wing model. The two dimensional PIV system consisted of a double-pulsed laser, optic lens, aerosol generator, high-speed camera, synchronizer, and corresponding software (Figure 6). An Nd:YAG laser with a pulse produced at 532 nm was used, which fulfills the intensity requirement to generate visible images of the flow field with micrometer-sized particles (mean oil droplet size of 1 μm generated from TSI 9307 oil droplet generator). This laser has a pulse width of less than 10 ns, which is short enough to avoid blurring after passing through the optical lens and splitting into thin sheets. The laser sheets were then oriented to the position that was perpendicular to the chord at 25%, 50%, 75%, and 100% wingspan by adjusting the laser and optical lens position (Figure 7). For the phase-lock process, the position of the pre-marked gear on the wing model was detected by the tachometer and a pulsed signal was transmitted to the synchronizer with a preset time delay. The synchronizer then sent out trigger signals to the high speed camera (PCO pixelfly, 1392×1040 pixels) which captured the flow structures. The time delay between two successive images was set at 130 μs. By synchronizing the time delay signal by the tachometer to the laser trigger, images in different fixed nondimensional time of one flapping cycle (Figure 1) were captured. At the same time, a signal was sent to the computer by the BNC board for reference of the trigger time. The force was measured simultaneously with the PIV system in order to quantify the flow characteristics at each phase-lock time. To eliminate noise, the average of 100 pairs of images was used in the flow visualization process. The interrogation window size for the PIV was 32×32 pixels. Fast Fourier transform (FFT)-based cross-correlation method is used and overlapping of 50% of the window size is applied. The PIV data processed by Insight 4G software have an uncertainty of less than 5%. Table 2 is a list of the equipment used in the experiment.

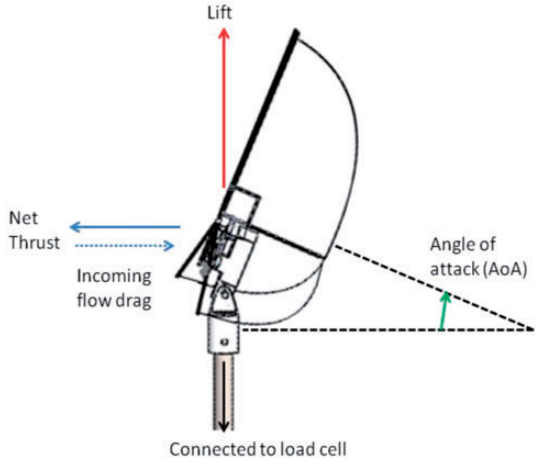

Figure 5. Schematic diagram of the force component on the wing model.

Results and discussion

Force measurement for level flight under freestream velocity of 2 m/s

The MAV was designed to fly at a low speed of less than 3 m/s. To fly at a horizontal flight, the drag encountered by these vehicles along the horizontal direction must be balanced by the average thrust that acts on these vehicles. An incoming flow of 2 m/s was introduced in the setup by placing the wing model into the wind tunnel. The coefficient of the net-thrust C_T is defined as

$$C_T = \frac{T - D}{0.5\rho V^2 S} \tag{2}$$

Table 2. List of equipment used in the PIV experiment.

Equipment	Company	Type	
Laser		QUANTEL	EverGreen
Delay generator	STANFORD	DG 535	
Synchronizer	BNC	Model 575	
A/D Board	National Instrument	BNC-2110 MIX	
Camera	PCO	Pixelfly	
Load cell	KYOWA	LSM-B-SA1	
Amplifier	KYOWA	WGA-800C	
Voltage data recording software	Dantec Dynamics	StreamWare	
PIV Software	TSI	Insight 4G	
Tachometer	Monarch	PLT200	
Oil droplet generator	TSI	9307	

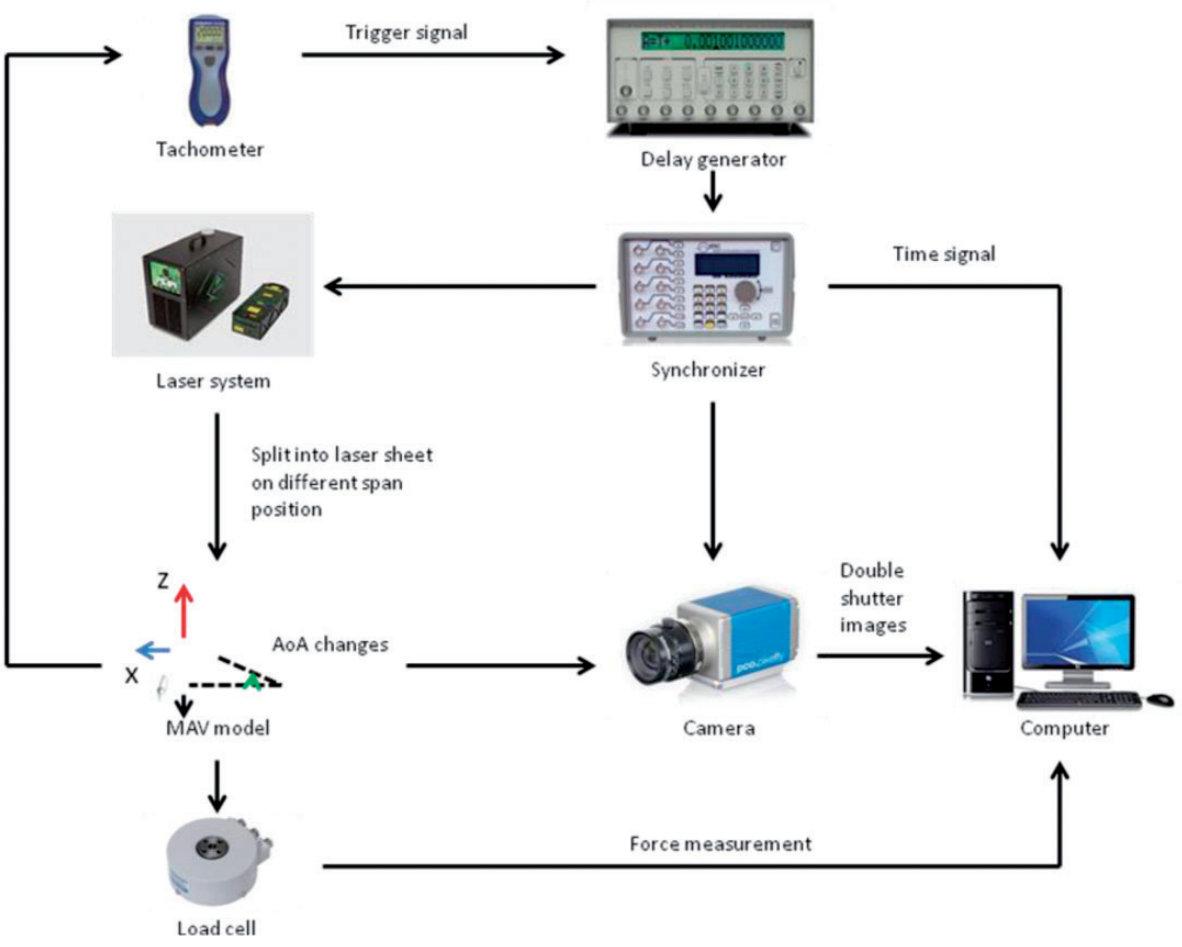

Figure 6. Flow chart of the PIV experiment setup.

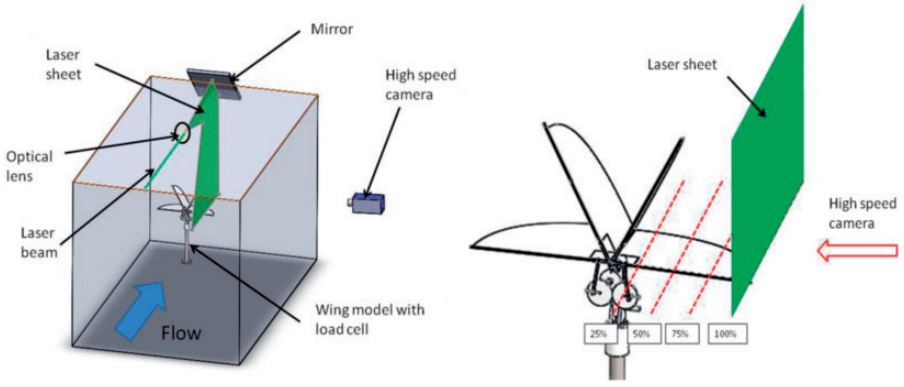

Figure 7. Schematic diagram of the PIV setup in wind tunnel (left) and the corresponding wing span positions of the laser light sheet on model in the PIV setup (right).

where T is the thrust that acts on vehicles, D is the drag encountered, ρ is the fluid density, and V and S are the true airspeed and wing surface area, respectively.

As shown in Figure 8, C_T at different tested AoA increases with flapping frequency. Besides, positive C_T is found at AoA lower than or equal to 30°, which indicates that the MAV can overcome drag and perform forward flight in those conditions.

The lift data of the selected AoA parameters are shown in Figure 9. Since the weight of the MAV is about 8 g, it is

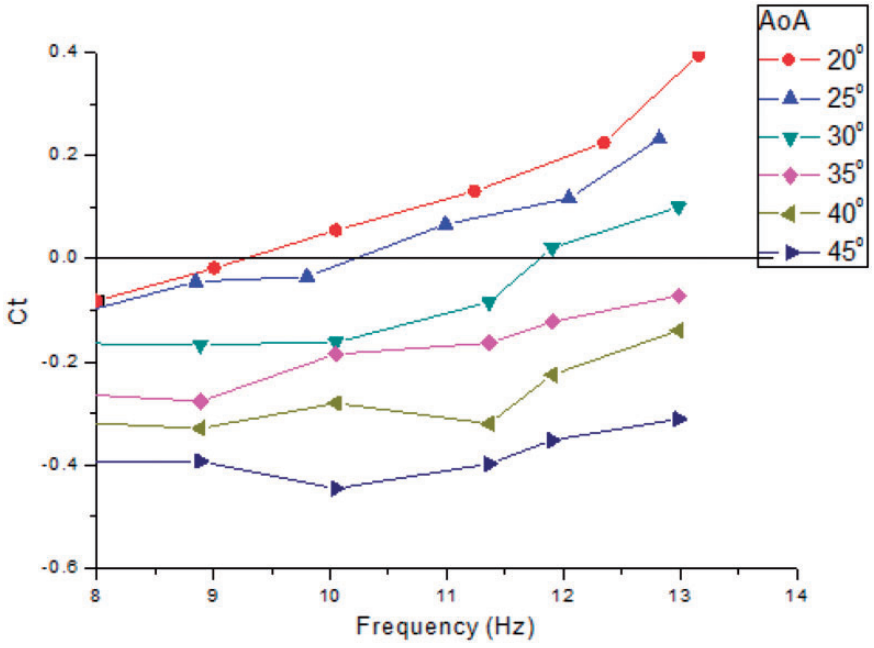

Figure 8. Relation of coefficient of thrust of flapping frequency at different AoA at a freestream velocity of 2 m/s.

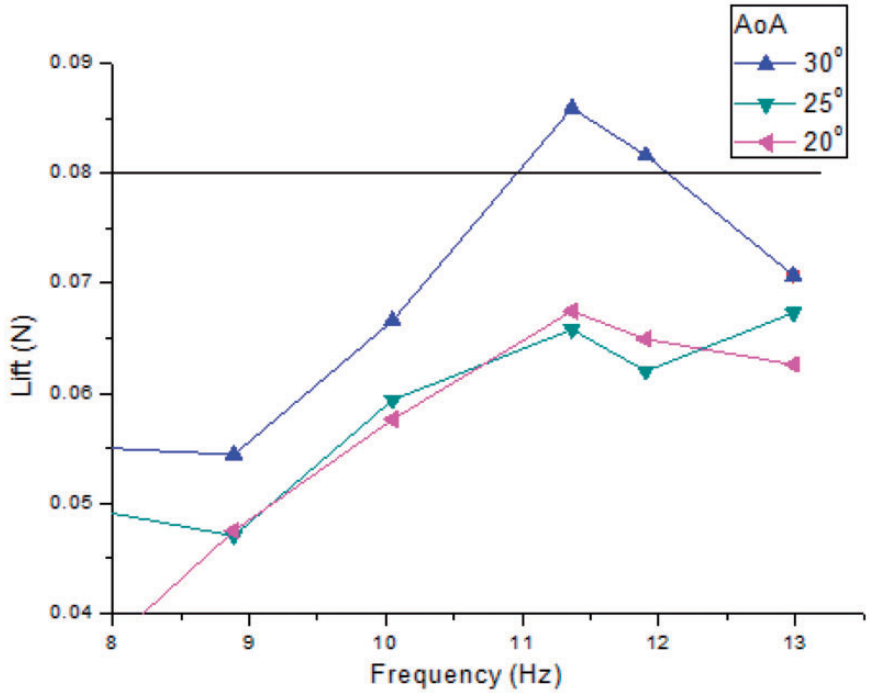

Figure 9. Relation of lift to flapping frequency at selected AoA with freestream velocity of 2 m/s.

assumed that at least 0.08 N of lift is generated by the flapping motion in real flight. The result indicates that in a condition where the AoA is 30° with a flapping frequency that ranges between 11 to 12 Hz, the MAV is capable of flying at a level flight of 2 m/s. Therefore, this condition is selected for study in the PIV experiment. The reason of lift drop after 11 Hz may due to the inconsistent wing deformation in high flapping frequency. Further studies will be conducted in the future. Figure 10 illustrates the lift variation during one flapping cycle under this condition and the characteristics will be discussed in the subsequent section together with the PIV result.

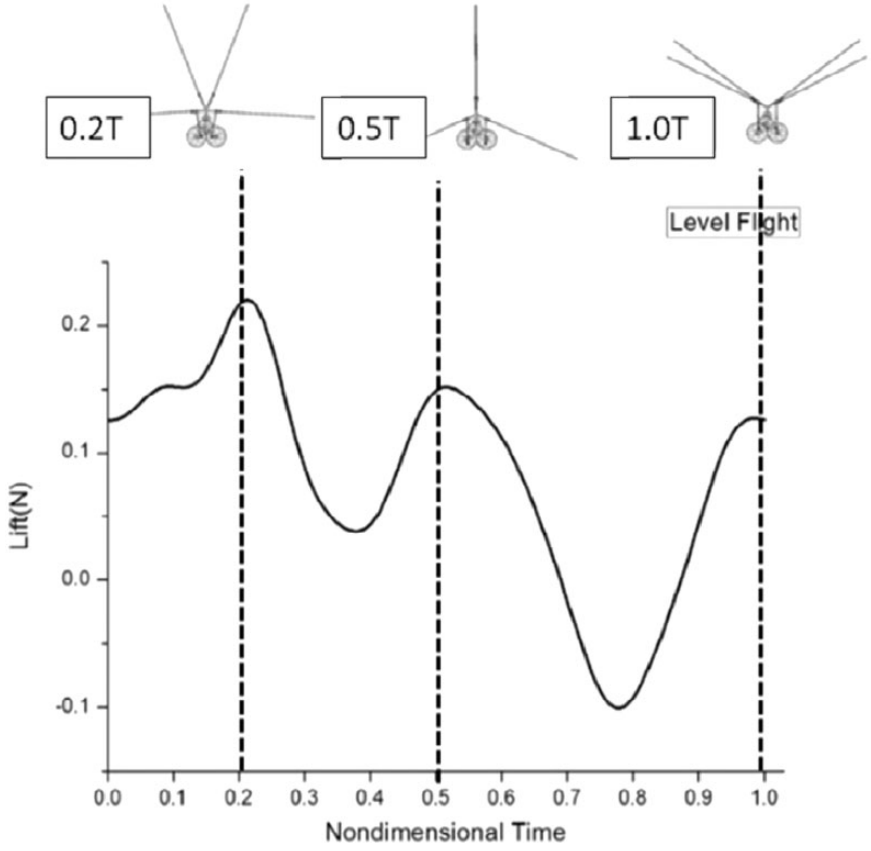

Figure 10. Typical lift variation in one flapping cycle at flapping frequency of 12 Hz and AoA of 30°.

Flow field behind the wingspan

The PIV measurements were performed at a free flow velocity of 2 m/s as stated in the previous section, with a flapping frequency of 12 Hz and AoA of 30°. At wingspan positions of 25%, 50%, 75%, and 100% from the wing root, 10 successive sets of images were captured. Figure 11 shows a comparison of the velocity magnitude behind the corresponding wingspan position at 0.0T/1.0T (refer to Figure 1) where the local lift maximum is found in Figure 10. Velocity magnitudes higher than 2 m/s are focused as the MAV cruises at that velocity in real forward flights. In order to provide a more detailed comparison of the induced velocity distribution, a characteristic location (i.e. wake behind the model at $x = 150$ mm) was selected behind the wingspan for each case and a velocity profile was extracted (Figure 12). The highest peak of the velocity magnitude was found behind 50% wingspan with a velocity that exceeds 2.5 m/s. In other words, a strong flow motion is more likely to be found at 50% wingspan. Therefore, the wake behind 50% wingspan at different fixed nondimensional times in each flapping cycle is selected for further examination (Figure 13).

At 0.0T (i.e. 1.0T) in Figure 13, a strong fluid jet is observed in the velocity map due to the clap motion of two sides of wings at that moment, which appears in the form of vortices with anti-clockwise rotation in the vortex evolution. The local lift maximum is found at that moment. Fling motion at the sides of two wings starts from 0.0T to 0.2T (Figure 1). With reference to the clap and fling mechanism in the MAV model, the leading edge is flung apart by rotation around the trailing edge at 0.1T, where the air rushes in to fill the gap between the two wings and a negative pressure is created.[22] The lift force produced reached to the maximum at 0.2T due to this fling motion as reflected on Figure 10. Since the fling happened between the two sides of wings, the strength cannot be reflected on velocity map at which the wake behind the span is the focus, and so no strong fluid jet is found at that moment. The positive vortex formed in 0.0T continues to move to a more distant position whereas a new positive vortex is formed right behind the wingspan at 0.2T. The new vortex grows around the trailing edge at 0.3T and moves outward at 0.4T, which is mostly due to the translational motion of the bottom wing against the free stream and the dissipation of the leading edge vortex. The clap motion is executed at 0.4T to 0.5T by the two center wings (Figure 1); however, the lift generated is less than that around 0.2T. Recalling the

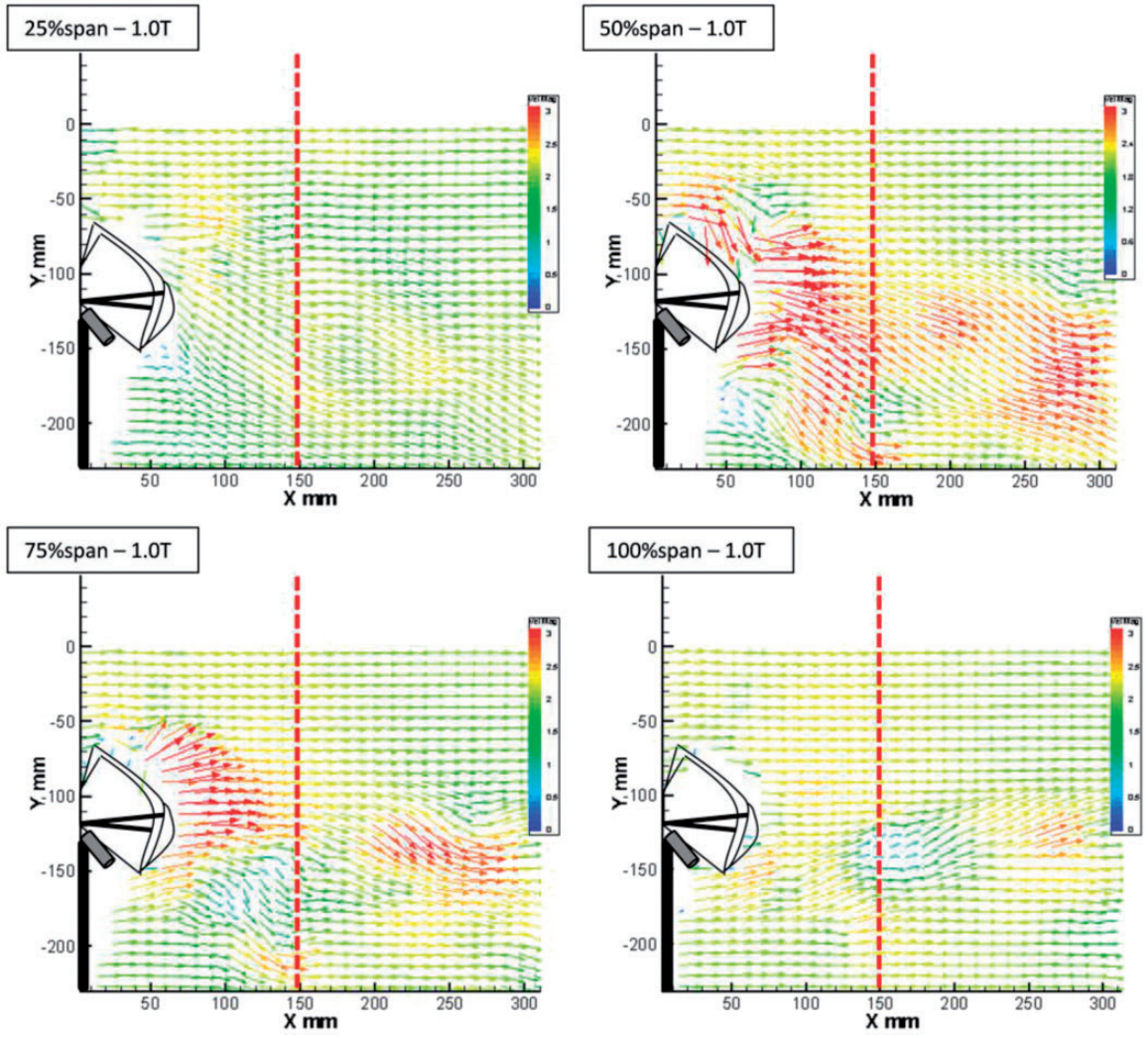

Figure 11. Flow topology behind 25%, 50%, 75%, and 100% wingspan at 1.0T.

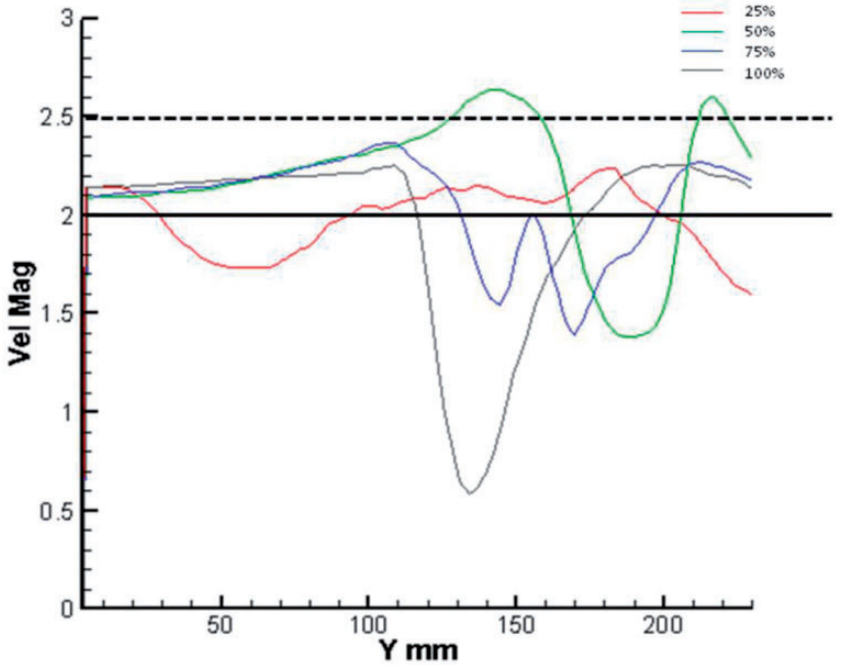

Figure 12. Relation of velocity magnitude to *Y* position at $X = 150$ mm in flow topology behind four wingspan positions at 1.0T.

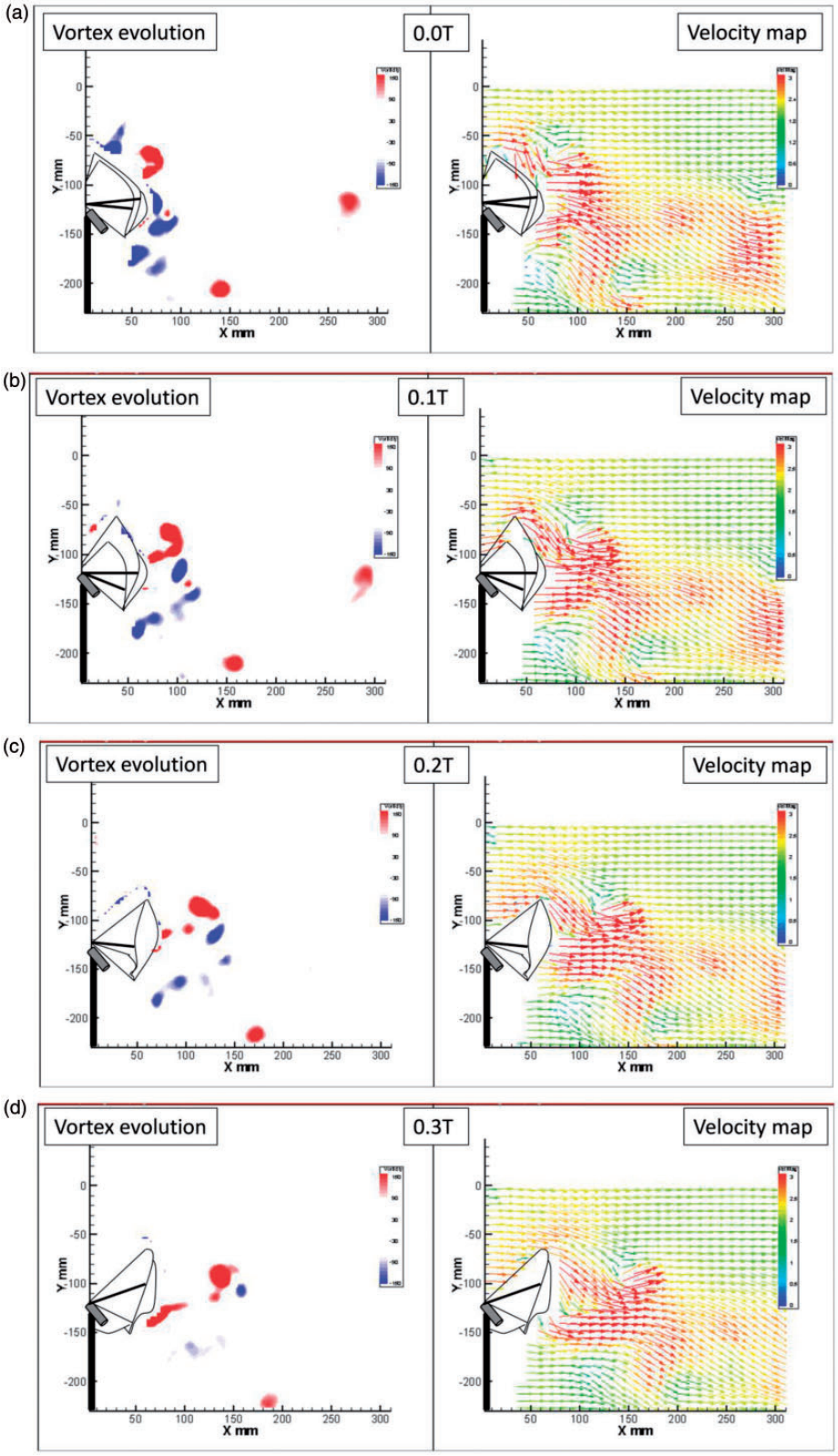

Figure 13. Vortex evolution (left) and velocity map (right) at the position behind 50% wingspan at (a) 0.0T, (b) 0.1T, (c) 0.2T, (d) 0.3T, (e) 0.4T, (f) 0.5T, (g) 0.6T, (h) 0.7T, (i) 0.8T, (j) 0.9T.

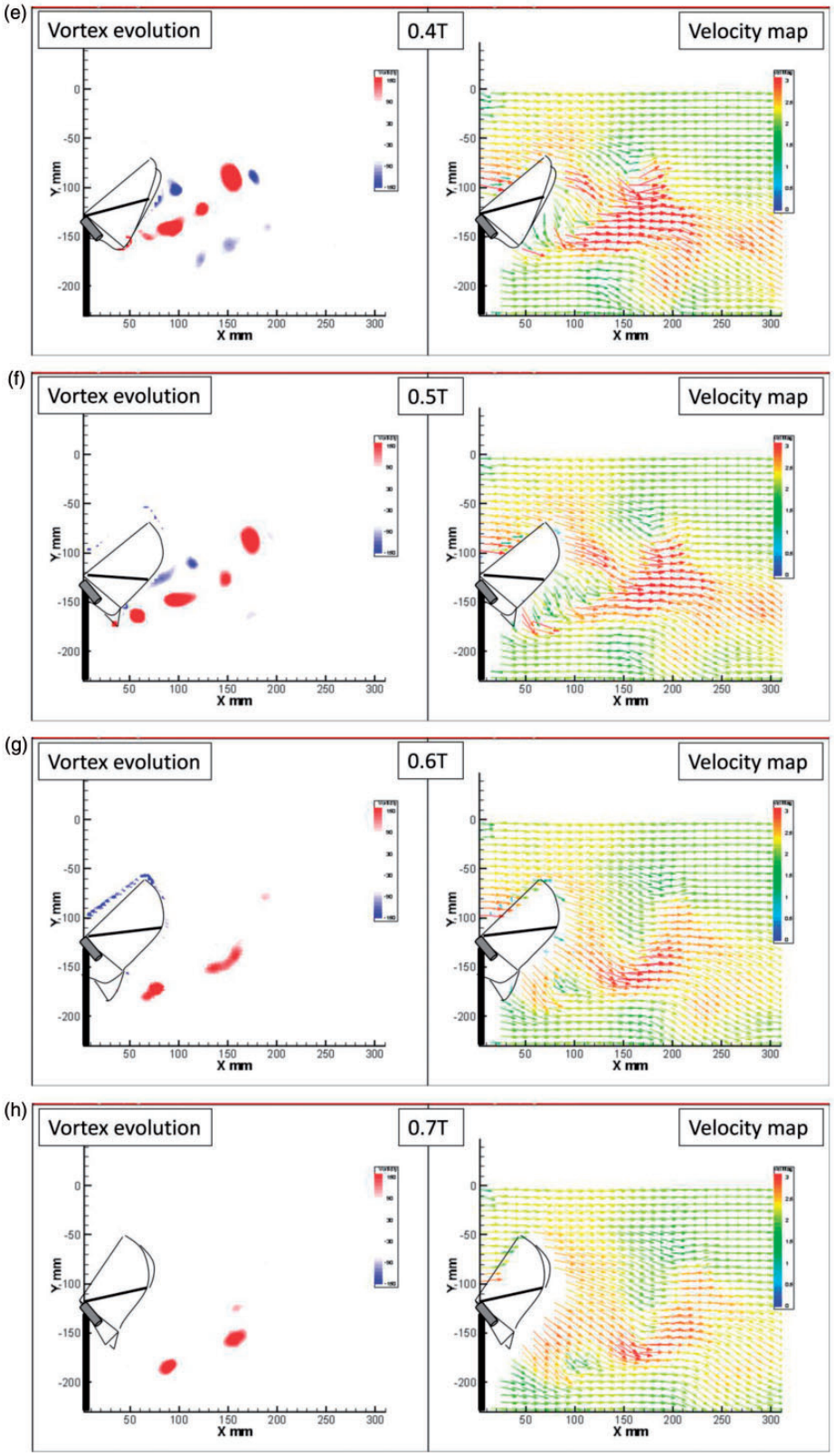

Figure 13. Continued.

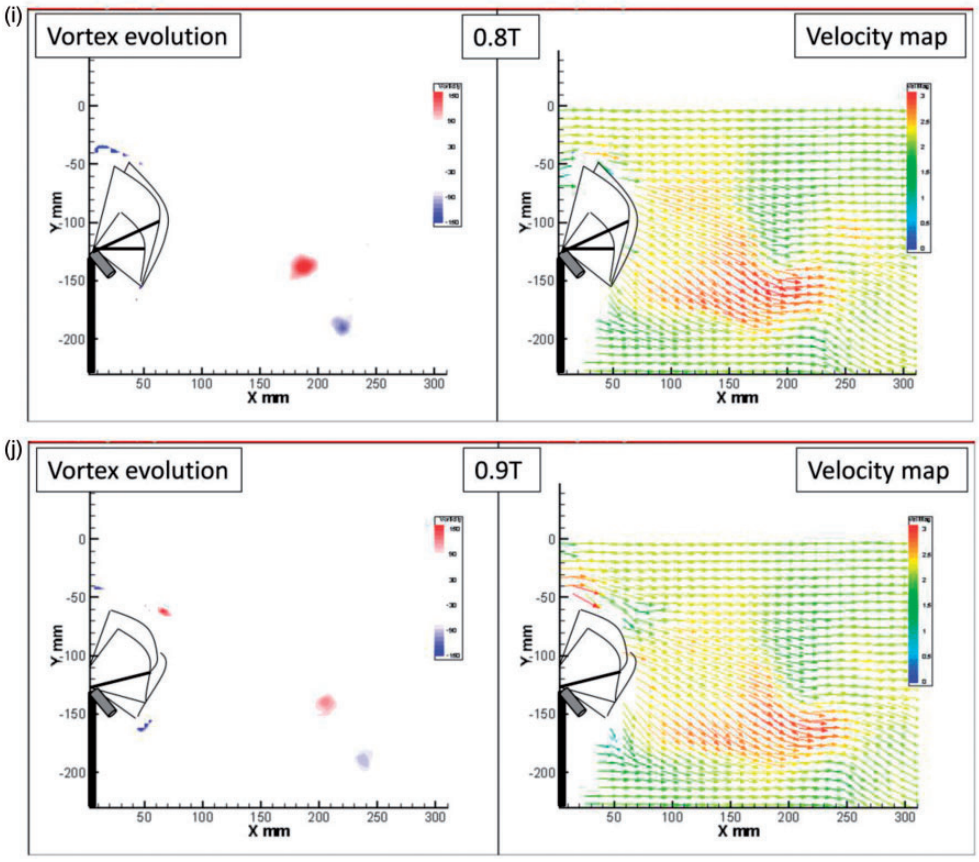

Figure 13. Continued.

biplane structure in the MAV model, it is not unusual that the fling motion at the two sides of the wings is much larger compared with the clap motion at the center wings only. The positive vortex keeps shedding from 0.5T to 0.7T but the strength is weaker compared with that in the first half of the flapping cycle. The fling motion between the center wings takes place at 0.8T, where the lift is expected to increase, but instead drops to the minimum level. The reason may be due to the initial momentum induced by the moving up of the lower wings. In observing the velocity vector direction at 1.0T behind 75% wingspan (Figure 11), upwash is found around the wings which might have already been generated at 0.6T and 0.8T, and this is responsible for the lift loss. No obvious vortex is shed after 0.8T in the flapping cycle.

Conclusion

To build a successful MAV model that can be applied for different purposes, both the design and aerodynamic considerations are important. In this research, a MAV model is built based on multiple components: frame structure, actuation, materials and flight control. Besides, the forward flight condition is verified by experiments and explained by aerodynamics.

First, a four-wing MAV model is made and tested for flight. The clap and fling mechanism is carried out in the current design with the use of a biplane structure. With the help of precision technology (i.e. MJM and EDM), the gears and frames are made and assembled by hand. A receiver board with actuators serves as the means of flight control for the model. The finished model has a weight of only 8 g and wingspan of 200 mm, and a flight test is conducted afterwards.

To investigate the forward flight condition in the air during the flight testing, the wing model is put under an incoming flow of 2 m/s in a wind tunnel. Both horizontal and vertical forces are measured at different AoA and flapping frequencies. Assuming that the MAV model is capable of flying forward at a speed no less than 2 m/s and capable of lifting its own weight, an AoA of 30° and flapping frequency of 12 Hz are concluded as the real forward flight conditions after the experiments are carried out, and these correspond to the flight test (video in section "Flight testing").

With the selected condition for the force measurement, the flow field at different wingspan positions and

different wing configurations is recorded by using the PIV system. With reference to the velocity map and the vortex evolution, the lift peaks at each flapping cycle are well explained with the clap and fling mechanism.

The study has revealed that the clap and fling mechanism plays a key role in the lift generation in our MAV model. Both an understanding of the MAV structures and the aerodynamics behind these structures are crucial in designing a flapping MAV.

Declaration of conflicting interests

The author(s) declared no potential conflicts of interest with respect to the research, authorship, and/or publication of this article.

Funding

The author(s) disclosed receipt of the following financial support for the research, authorship, and/or publication of this article: This study was supported by Innovation and Technology Commission, Hong Kong under Contract No. ITS/045/13 and by Department of Mechanical Engineering, The Hong Kong Polytechnic University under Departmental General Research Fund G-UB49.

References

1. Liu T. Comparative scaling of flapping- and fixed-wing flyers. *AIAA J* 2006; 44.
2. Sane SP. The aerodynamics of insect flight. *J Exp Biol* 2003; 206: 4191–4208.
3. Warrick DR, Tobalske BW and Powers DR. Aerodynamics of the hovering hummingbird. *Nature* 2005; 435: 1094–1097.
4. Lehmann FO, Sane SP and Dickinson M. The aerodynamic effects of wing-wing interaction in flapping insect wings. *J Exp Biol* 2005; 208: 3075–3092.
5. Weis-Fogh T. Quick estimates of flight fitness in hovering animals, including novel mechanisms for lift production. *J Exp Biol* 1973; 59: 169–230.
6. Truong TV, Byun D, Kim MJ, et al. Aerodynamic forces and flow structures of the leading edge vortex on a flapping wing considering ground effect. *Bioinsp Biomim* 2013; 8036007.
7. Nakata T, Liu H, Tanaka Y, et al. Aerodynamics of a bio-inspired flexible flapping-wing micro air vehicle. *Bioinsp Biomim* 2011; 6045002.
8. de Croon GCHE, de Clercq KME, Ruijsink R, et al. Design, aerodynamics, and vision-based control of the DelFly. *Int J Micro Air Veh* 2009; 1: 71–97.
9. Pornisn-sirirak TN, Tai YC, Nassef H, et al. Titanium-alloy MEMS wing technology for a micro aerial vehicle application. *Sens Actuat A* 2001; 89: 95–103.
10. Nguyen QV, Park HC and Goo NS. A flying insect-like flapper actuated by a compressed LIPCA. In: *Proceedings of the 2007 IEEE international conference on robotics and biomimetics*, Sanya, China, 2007.
11. Jones KD, Bradshaw CJ, Papadopoulos J, et al. Bio-inspired design of flapping-wing micro aerial vehicles. *Aeronaut J* 2005; 109: 385–393.
12. Banala SK and Agrawal SK. Design and optimization of a mechanism for out-of-plane insect wing like motion with twist. *J Mech Des/Trans ASME* 2005; 127: 841–844.
13. McIntosh SH, Agrawal SK and Khan Z. Design of a mechanism for biaxial rotation of a wing for hovering vehicle. *IEEE/ASME Trans Mechatron* 2006; 11: 143–153.
14. Heathcote S, Wang Z and Gursul I. Effect of spanwise flexibility on flapping wing propulsion. *J Fluids Struct* 2008; 24: 183–199.
15. Yusoff H, Abdullah MZ, Abdul Mujeebu M, et al. Effect of skin flexibility on aerodynamic performance of flexible skin flapping wings for micro air vehicles. *Exp Techniq* 2012; 39: 11–20.
16. Wu P, Ifju P and Stanford B. Flapping wing structural deformation and thrust correlation study with flexible membrane wings. *AIAA J* 2010; 48.
17. Hu H, Gopa Kumar A, Abate G, et al. An experimental investigation on the aerodynamic performances of flexible membrane wings in flapping flight. *Aerosp Sci Technol* 2010; 14: 575–586.
18. Mahardika N, Nguyen QV and Park HC. Effect of outer wing separation on lift and thrust generation in a flapping wing system. *Bioinspir Biomim* 2011; 6036006.
19. Apker TB and Corke TC. Experiments and modeling of micro flapping wings of different designs in hover. *AIAA J* 2015; 53: 542–553.
20. Isaac KM, Rolwes J and Colozza A. Aerodynamics of a flapping and pitching wing using simulations and experiments. *AIAA J* 2008; 46: 1505–1515.
21. Truong QT, Nguyen QV, Park HC, et al. The dynamics characteristics of LIPCA and its application for mimicking insect flapping motion. In: *IEEE/RSJ international conference on intelligent robots and systems*. Nice, France: Acropolis Convention Center, 2008.
22. Huang SK, Cairo R, Parker R, et al. An experimental investigation on wing optimization for a four-wing flapper. In: *51st AIAA aerospace sciences meeting including the new horizons forum and aerospace exposition*. Grapevine, Texas: Gaylord Texan Hotel and Convention Center, 2013.
23. Combes SA and Daniel TL. Flexural stiffness in insect wings II. Spatial distribution and dynamic wing bending. *J Exp Biol* 2003; 206: 2989–2997.